INFRAGRAVITY PERIOD OSCILLATIONS IN A CHANNEL HARBOR NEAR A RIVER MOUTH

Florian Bellafont[1], Denis Morichon[2], Volker Roeber[3 4], Gaël André[5], Stéphane Abadie[6]

Port of Bayonne, located in SW France, is a channel harbor situated near the river mouth of the Adour. Long-period oscillations have repeatedly caused snapping of mooring lines of berthed ships and have led to wave resonances in an adjacent marina (seiche). To investigate mechanisms for generation of theses oscillations, a field campaign was carried out during a one-year return-period storm (Hs = 6 m and Tp = 15 s): four pressure sensors were deployed inside the port. To complement the data and to better understand the governing processes that lead to the wave transformations in Port of Bayonne, the storm event was computed with the Boussinesq-type model, BOSZ.
The data confirm the model results, which show generation of long infragravity (IG) waves by the incident swell around the harbor entrance and free propagation of these waves without amplification over far distances inside Port of Bayonne. Excited by these long waves, resonance oscillations are only noticeable in a small enclosed marina. Though the IG-waves are not causing substantial changes to the water level along the harbor channel, they are suspected to excite the ships' eigen modes, which consequently results in mooring problems.

Keywords: channel harbor; harbor oscillation; infragravity waves; Boussinesq model; BOSZ; surf zone processes; long waves; wave spectrum

INTRODUCTION

Harbor entrances are usually designed for protection against wind and swell waves with periods ranging between 5 s and 20 s. However, many harbors experience agitation problems caused by long waves with periods longer than 30 s. In most cases, a harbor is a semi-enclosed water basin located on the coast and therefore an oscillating system. When the period of external forcing is close to the eigen periods of the basin, resonance occurs. With energetic external forcing, a standing wave, associated with vertical oscillations and strong currents, develops: this phenomenon is called coastal seiche (Rabinovich, 2009).

A stationary system of coastal seiche can hardly develop in river ports, because there is no upstream boundary on which a wave can be reflected. In addition, infragravity waves (IG), when entering the river, can excite the system constituted by the ship at dock and its mooring lines (Van Der Molen et al., 2006). IG waves are long surface waves with periods between 30 s and 300-600 s (5-10 min) and are generated by two main mechanisms (Bertin et al., 2018): non-linear interactions between short waves generate an IG wave which travels phase-locked to the wave groups and is called bound wave (Longuet-Higgins and Stewart, 1962). In addition, the temporal variation of the breaking zone causes a time-variation of the wave set-up and generates free long waves (Symonds et al., 1982).

Different classes of wave models can be used to simulate the transformation of nearshore waves and their interaction with coastal structures. Spectral wave models are usually applied to describe the characteristics of short waves at the toe of a structure. They include the effects of refraction and breaking processes on wave transformation but they are not adapted to precisely describe wave diffraction by coastal structures which is dominant in harbour environment (Booij et al., 1997; Tolman et al., 2009). The models based on the mild slope equations, also called Berkhoff model, allow to overcome this limitation by solving explicitly both refraction and diffraction processes for waves propagating over a gentle slope (Berkhoff, 1973). The mild slope equations were derived for combined refraction and diffraction of linear periodic waves. They are well adapted to describe the interaction of long waves with port structures. They were used in numerous studies to numerically investigate the oscillation of port basins induced by long wave forcing and the conditions for seiche generation (Lee and Xing, 2010; Okihiro et al., 1993; Thompson and Hadley, 1995). Boussinesq-type wave models are well suited to simulate the impact of storm waves on harbour oscillations. They allow to simulate both short and long wave interactions with port structure (Thotagamuwage and Pattiaratchi, 2014b; Guerrini et al., 2014; Gierlevsen et al., 2001).

This study aims to study the oscillation in the Port of Bayonne (France) by combining water elevation measurements and numerical simulations results. This port, located near the mouth of the Adour River,

[1]SIAME EA 4581, University of Pau and Pays de l'Adour, France
[2]SIAME EA 4581, University of Pau and Pays de l'Adour, France
[3]E2S Chair HPC-Waves, University of Pau and Pays de l'Adour, France
[4]Univ of Hawaii at Manoa, Dpt of Oceanography, USA
[5]Hydrographic and Oceanographic Service of the Navy (SHOM), France
[6]SIAME EA 4581, University of Pau and Pays de l'Adour, France

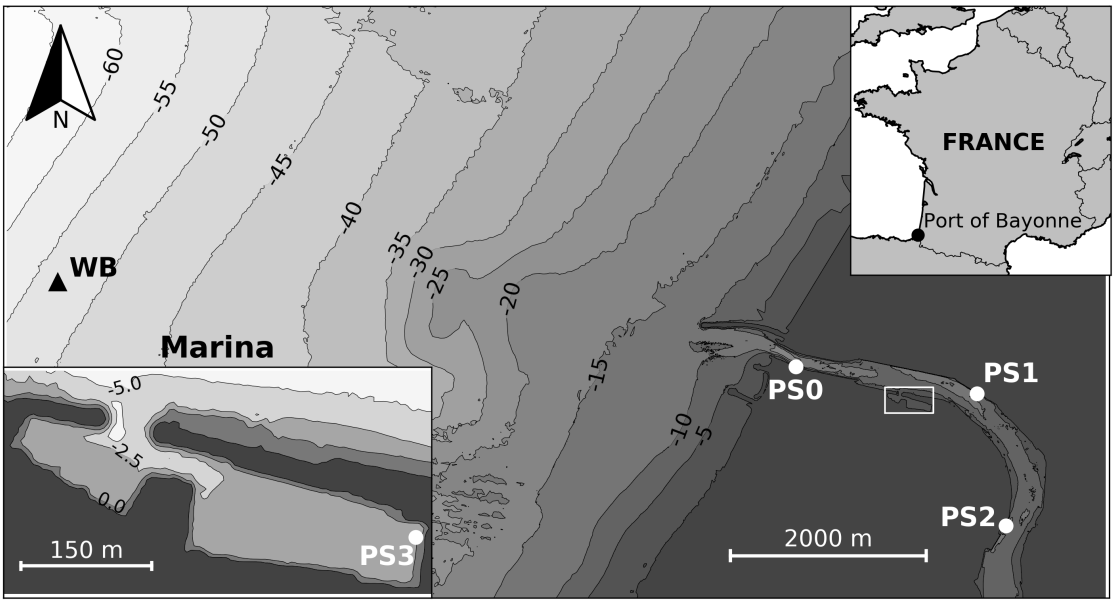

Figure 1: Port of Bayonne and positions of the experimental devices: WB waverider buoy, and PS pressure sensors (white dots): PS0 (river mouth), PS1-PS2 (channel and commercial harbor) and PS3 (marina). Zoom on the marina in the lower left corner (white rectangle on the map).

frequently faces problems in keeping boats docked during storm conditions and long-period oscillations have led to resonance of an adjacent marina. A field campaign was carried out during a storm event (Hugo) that occurred around March 23, 2018. Offshore wave conditions were typical of a one-year return-period storm (Hs = 6 m and Tp = 15 s) (Abadie et al., 2005). The data collected during this event are used both to characterize the oscillations inside the harbor and the marina and to validate a numerical wave model based on the Boussinesq equations. The model is used to complement the measurements by providing information about the generation processes of IG waves outside the harbor and their behavior inside the river and the marina.

STUDY SITE

Port of Bayonne is located on the south-western shore of France in the Adour river (figure 1). It is composed by two harbors: a channel and commercial harbor that extends up to 6.5 km upstream of the river with an average depth of 14 mCD with respect to chart datum which corresponds to the lowest astronomical tide level. A marina (Port of Brise-Lames), a semi-enclosed water basin with an average depth of 2.5 m, is located on the left shore, 1.4 km from the river mouth. The minimum, average and maximum annual river flow of the Adour are respectively 30, 300 and 2000 m^3/s. Two breakwaters protect the entrance of Port of Bayonne from lateral currents and swell waves. An underwater sediment deposit made of material from dredging operations of the river is located between 2.5 and 3.5 km from the coast. The minimum depth above the deposit reaches 17 m. The tidal regime of the area is mesotidal with a mean sea level (MSL) and a tidal range during spring tides of 2.53 m and 3.5 m respectively.

DATA AND METHODS

A directional wave buoy, moored in 50 m water depth at 5.3 km from the coastline, records offshore wave conditions and provides a sea and swell directional spectrum every 30 min. The Adour river flow is obtained from the Banque Hydro data base (hydro.eaufrance.fr), and the atmospheric pressure is hourly measured by a weather station located in Biarritz. Four pressure sensors, with a sampling frequency of 1 Hz, were deployed in Port of Bayonne during a storm event. Three sensors were fixed in the channel harbor at 0.3, 2.2 and 3.7 km from the river mouth, and one in the marina (figure 1).

The pressure data are transformed into free surface time series by applying the hydrostatic pressure for-

mula whose application range is respected, since the sensors are located outside the surf zone and installed near the free surface at a depth of 1.5 m (Bonneton and Lannes, 2017).

A spectral analysis of the free surface elevation time series was performed to study the energy distribution in the different frequency bands as well as their spatial and temporal evolution. After removing the tidal contribution by considering a linear deviation of the signal, the significant height (Hs) is calculated from series of 2048 water level data (~34 min) according to the formula (1) (Holthuijsen, 2010).

$$Hs = 4\sqrt{m_0} \tag{1}$$

where Hs refers to the significant wave height and m_0 to the zeroth-order moment of the spectrum.

Free surface oscillations in the period bands of short (5-30 s) and infragravity (30-300 s) waves can be determined by fixing the integration bounds of m_0. The power spectral density of the free surface is determined by dividing the signal into 2048 data segments with a 50% overlap between each segment and applying a Hanning window. The mean spectrum being related to the variance of the free surface, the associated confidence interval (CI) follows a Chi-square law (χ^2) (Thomson and Emery, 2014).

$$CI = \left[\frac{\nu.s^2}{\chi^2_{\alpha/2,\nu}}; \frac{\nu.s^2}{\chi^2_{1-\alpha/2,\nu}}\right] \tag{2}$$

where ν denotes the degree of freedom equal to the number of segments minus 1, s^2 the calculated variance and α the confidence coefficient taken at 5%.

NUMERICAL MODEL

The propagation of the waves from the wave buoy to the Adour river during storm Hugo is simulated with the BOSZ numerical model (Roeber et al., 2010; Roeber and Cheung, 2012). It is a Boussinesq-type model based on the equations of Nwogu (1993) expressed in conserved variable formulation. The numerical solution utilizes a low-diffusion Finite Difference scheme for the propagation of the waves towards the surf zone and a robust, shock-capturing Finite Volume scheme for wave breaking and moving boundary (wet/dry) processes.

Model setup

The numerical domain extended 8 km seaward to include the offshore wave buoy (50 mCD of water depth), and covered 8.5 km of coast (centered on the harbor mouth). The upstream boundary is far enough from the area of interest to limit boundary disturbances (figure 2). A sponge condition is applied at the domain boundaries except at the upstream river boundary where a radiation condition is applied to allow for long waves to leave the domain. The mesh is composed of square cells, of which ~50% are wet. Two grid resolutions are chosen, 6.5 and 10 m, to study the effect of mesh size in terms of computation time and convergence of the results (table 1). With a 20˚clockwise rotation of the domain, the western boundary is oriented perpendicular to the peak direction of the incoming swell. The seabed material in the study area is essentially fine sand with some mud deposits in the river. Rocky outcrops have been identified 2 km south of the mouth of the Adour River (Augris and Clabaut, 2001). Based on this information, a uniform Manning roughness coefficient of 0.015 s/m^3 was applied to the entire domain, corresponding to sand grain with diameter 0.3 mm (Arcement and Schneider, 1989). A factor of 10 is applied to the cells covered by the harbor breakwater to take into account their effect on short waves dissipation due to their rubble-mound armor layers.

The model simulation period is 4 hours, the first 30 minutes are used to ramp up the model and ensure a fully developed wave field. The remaining 3h30 are divided into 30 min segments and their power spectral densities are averaged. Since no phase information is provided in the input spectrum, the BOSZ model assigns a random phase to each spectral component and therefore multiple simulations are required to rule out particular wave-wave interactions due to the set of random wave phases (see (Roeber and Bricker, 2015)). Since the Boussinesq-type equations have only limited dispersion capabilities, the input wave spectrum is truncated near the high-frequency tail. The BOSZ model uses the ratio of wavelength to water depth (μ) to set the threshold of the high frequency tail. The truncated energy is redistributed over the remaining frequency bins to maintain the overall energy of the spectrum. The ratio $\mu = 1.5$ was found appropriate, thus waves with a period of less than ~7 s are not included in the input spectrum (at a depth of 50 m and applying the linear dispersion relation (Holthuijsen, 2010)). Since the individual waves are

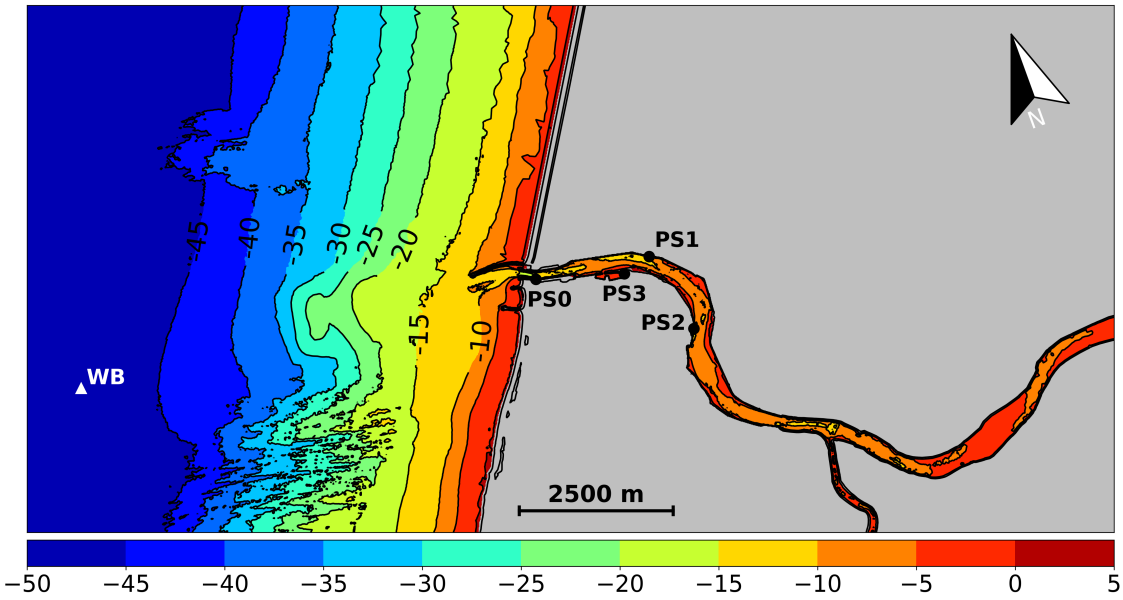

Figure 2: Numerical domain and numerical sensor locations. The first 100 offshore cells are flat. Wet cells are in grey.

Table 1: Numerical domain characteristics and computational time.

Grid resolution	m	**10**	**6.5**
Cells	millions	1.5	3.5
Wet cells	%	49	47
Computational time	days	1	3.5
12 cores: Intel Xeon x5675 @ 3,06 GHz			

generated for a specific water depth, the bathymetry along the wavemaker is of uniform 50-m depth without friction covering about 100 offshore cells.
It is important to notice that the truncation of the input spectrum only affects the waves, which are generated as input. The governing equations are not affected by this method. Essentially, waves of any length - as long as they can be numerically accounted for over the grid - are free to evolve during the computation; e.g. high frequency waves often result in form of super-harmonics of the main carrier frequencies from the shoaling process.

Selected event

The effects of river flow and tide are neglected. To respect this hypothesis, the numerical study focuses on the event of 24 March 2018 from 14:30 to 15:00 (UTC) at low tide: the mean water level was 1.97 mCD with a standard deviation of 0.05 m, and the Adour flow (430 m^3/s) was slightly higher than the mean annual river flow. The wave characteristics measured offshore were : Hs, peak period (Tp), direction at the peak and directional spreading at the peak equals to 5.7 m, 18 s, 299°and 19°respectively. The BOSZ model is forced with a frequency-direction spectrum reconstructed from wave buoy measurements using a parametric directional spreading function (team et al., 2007).

RESULTS

Field data

During the storm event, from 24 to 25 March 2018, the offshore significant wave height and peak period reached maximum values of 6 m and 18 s respectively. Figure 3 shows the response of Port of Bayonne to external forcing: Hs in the channel harbor (b) and in the marina (a). The contribution of short waves (5-30 s) in harbor oscillations is low ($Hs_{SW} < 0.15\ m$) unlike IG waves whose significant heights Hs_{IG} reach

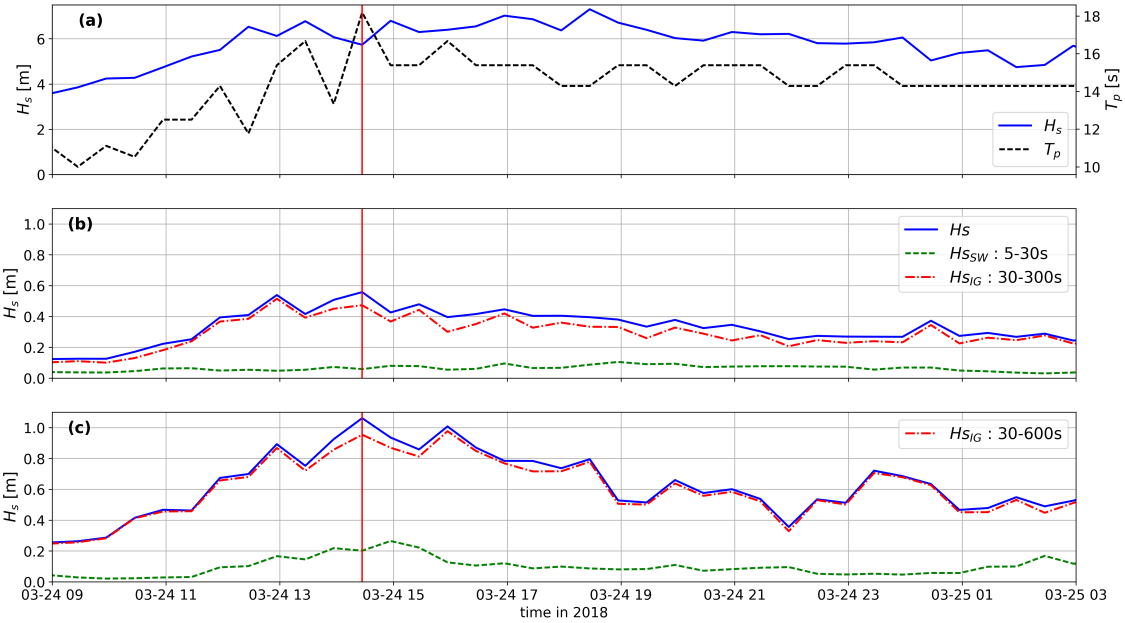

Figure 3: Storm event: (a) Hs and Tp at the offshore wave buoy ; (b) Hs in the channel harbor (PS1) and (c) Hs in the marina (PS3). The red vertical line corresponds to the simulated event.

values of 0.47 m for an Hs of 0.55 m in the channel harbor and an Hs_{IG} of 0.95 m for an Hs of 1.07 m in the marina. The period band of Hs_{IG} has been extended to 600 s for the marina in order to include the period of basin's fundamental mode (see power spectral density figure 4).

To study the waves transformation during the propagation in the river, power spectral densities (PSD) at the pressure sensors are presented in figure 4 (18h of data). From these densities, significant wave heights are calculated and the contribution of the different period bands to the variance of the free surface is expressed as a ratio of m_0 ($R_{SW} = m_{0,SW}/m_0$) (table 2). A significant part of the short waves energy is dissipated by the breakwaters: despite an Hs greater than 5 m at the wave buoy, Hs_{SW} is equal to 1 m at the Port mouth (PS0). In the port, the remaining energy dissipates quickly and its contribution to the variance of the free surface is low: $Hs_{SW} < 0.10\ m$ and $R_{SW} < 5\%$ for PS1 to PS3. The contribution of IG waves to the variance of the free surface is rather low (~30%) at the Port mouth (PS0) but Hs_{IG} is equal to 0.7 m. In the channel harbor, the IG energy is very high ($R_{IG} > 80\%$) and dissipates slightly: only 6 cm in terms of Hs between PS1 (2.2 km) and PS2 (3.7 km), i.e. 20% dissipation. The very long waves (VLW), with a period between 300 and 600 s, have a weak part in the channel harbor oscillations: $Hs_{VLW} < 0.15\ m$ and $R_{VLW} < 6\%$ for PS0-PS2.

In the marina (PS3), the PSD has several peaks that are characteristic of amplification by basin geometry and correspond to the eigen mode periods of the marina (semi-closed configuration) (Thotagamuwage and Pattiaratchi, 2014a). These periods can be estimated by applying the Merian formula (Raichlen, 1966). The main peak is related to the fundamental (Helmholtz) mode with period of 330 s, a broad peak is visible at 125 and 80 s, and three peaks are more marked at 45, 27 ans 22 s. The marina geometry causes an amplification of the external forcing, thus an increase of Hs: $Hs_{IG} = 0.50\ m$ and $Hs_{VLW} = 0.30\ m$.

Measurement and model result comparison

The power spectral densities from the measured and simulated water level time series are presented in figure 5 for the channel harbor and in figure 6 for the marina.

At PS0, short waves energy is globally underestimated and particularly for periods of less than 12 s. This can be due to the effect of local wind not taken into account in the model and to the cut-off period of 7 s on the input spectrum. For the other sensors (PS1 and PS2), the energy in short wave period band is very low and can neglected: $Hs_{SW} < 0.05\ m$.

Spatial variation and frequency distribution of IG waves (30-300 s) are well reproduced by the model

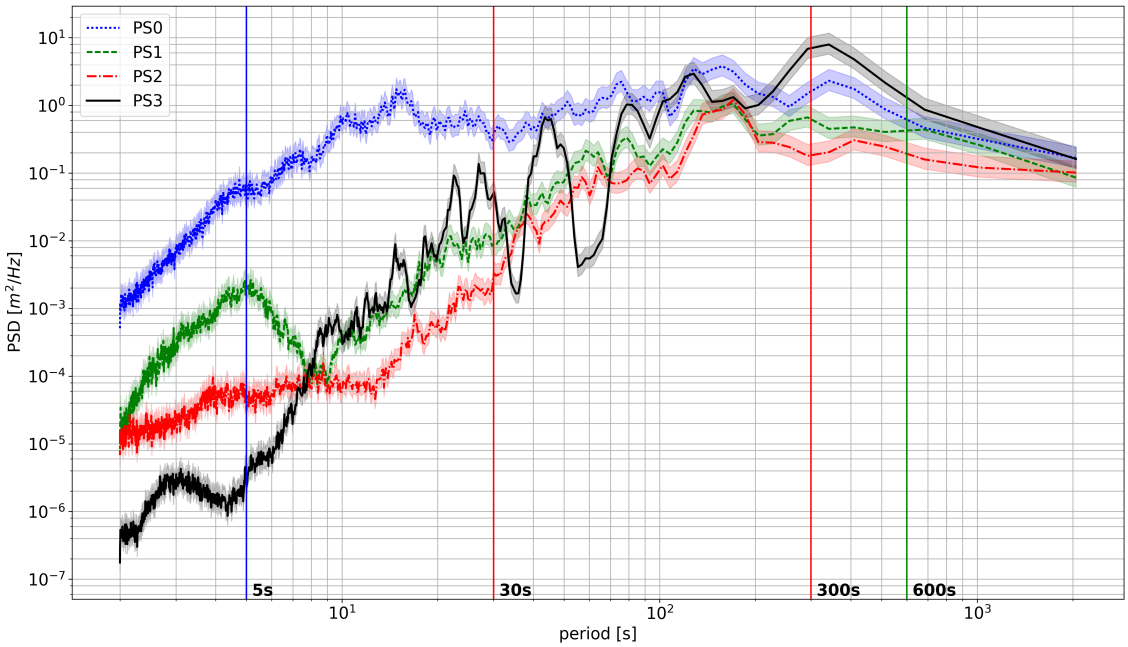

Figure 4: Power spectral densities (PSD) at pressure sensors and confidence intervals (CI).

Table 2: Hs in different period bands calculated from PSD (figure 4) and contribution (R) of the different period bands to the variance of the free surface.

	Hs	**SW**		**IG**		**VLW**	
		5-30s		30-300s		300-600s	
	m	Hs (m)	R (%)	Hs (m)	R (%)	Hs (m)	R (%)
PS0	1.28	0.99	61	0.72	32	0.16	2
PS1	0.35	0.07	4	0.31	79	0.08	6
PS2	0.27	0.02	1	0.25	86	0.06	6
PS3	0.67	0.12	3	0.53	62	0.28	17

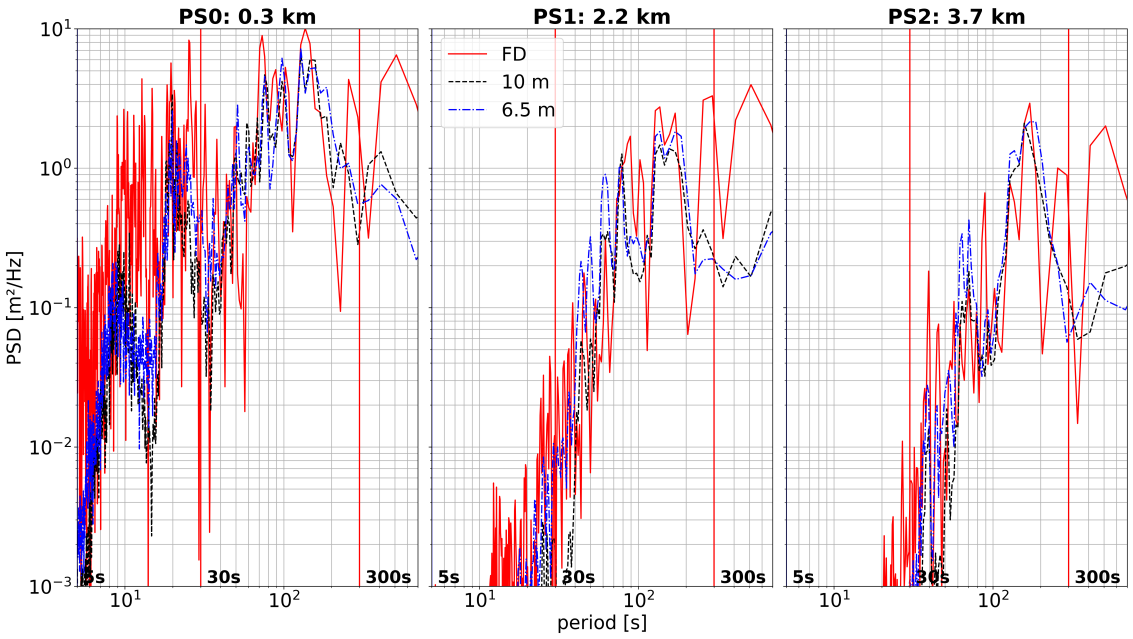

Figure 5: Power spectral densities for measured (FD) and simulated data with the two grid resolutions (10 and 6.5 m), in the channel harbor (PS0 to PS2).

Table 3: Hs in different period bands calculated from PSD (figures 5 and 6).

	Hs			**SW (5-30 s)**			**IG (30-300 s)**				
				Hs (m)			Hs (m)			Diff (%)	
	Meas.	6.5m	10m	Meas.	6.5m	10m	Meas.	6.5m	10m	6.5m	10m
PS0	1.62	1.06	1.00	1.22	0.63	0.57	0.94	0.83	0.79	-12	-17
PS1	0.56	0.44	0.38	0.06	0.03	0.02	0.47	0.42	0.35	-12	-25
PS2	0.37	0.36	0.30	0.02	0.01	0.01	0.31	0.34	0.29	10	-7
PS3	1.06	0.68	0.56	0.20	0.05	0.01	0.77	0.62	0.49	-19	-37

for the channel harbor sensors (PS0 to PS2) and for the two grid resolutions (6.5 and 10 m): the shape of computed spectral energy from BOSZ agree well with the measurements. But, the underestimation of spectral energy for periods higher than 290 s results in a 10% difference in the Hs_{IG} values for the 6.5 m mesh size and for the sensors in the channel harbor (underestimation for PS0 and PS1, and overestimation for PS2): the differences of Hs_{IG} are from 0.03 m to 0.10 m. For the 10 m mesh size, the Hs_{IG} values are underestimated by about 20% for PS0 and PS1 and 10% for PS2: the differences of Hs_{IG} are from 0.03 m to 0.15 m.

At PS3 (the marina), the 45 s peak is well reproduced by the model as well as the broad peak between 50 and 200 s. The underestimation of energy at peaks at 290 and 450 s results in significant differences of Hs_{IG}: 20% and 40% for 6.5 and 10 m grid resolution respectively. The sensor PS3 is used to study the impact of the mesh size on simulation results, as the width of the channel between the two basins is 50 m (figure 1). The spectral energy differences between the two meshes are small for periods greater than 40 s.

Comparisons of spectra in the IG period band show that the BOSZ model can reproduce the generation of IG by ocean forcing and their transformation during propagation in the river.

Local nearshore bathymetry effects

The significant wave height is determined at each point of the mesh using the formula 3 (Holthuijsen, 2010).

$$Hs = 4\sigma_\eta \tag{3}$$

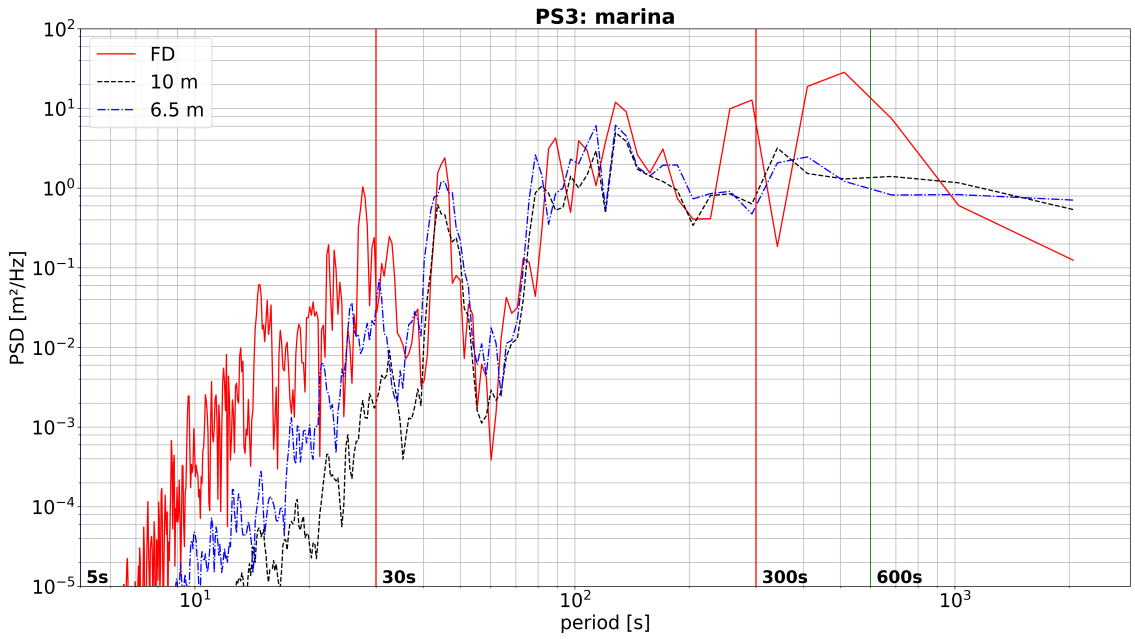

Figure 6: Power spectral densities for measured (FD) ans simulated data with the two grid resolutions (10 and 6.5 m), in the marina (PS3).

where σ_η is the standard deviation of the free surface elevation η.
Thus, only two sums are stored and updated at each time iteration: η and η^2 and not all the time series.

Hs map is presented in figure 7 in the port mouth area for 10 m grid resolution. With the bathymetry contour lines, the deposit of dredged material is visible at depths between -35.0 and -17.5 mCD. To study its effects on waves transformation, it is removed from the domain and replaced by an uniform slope (the initial bathymetry), all other simulation parameters are the same. The differences of Hs with and without the deposit are in figure 8.

The reduction in water depth by the deposit causes the shoaling of incident waves: Hs increases, the free surface steepens, and non-linearity increases with the possibility of IG waves generation. In addition, the deposit causes the concentration of energy on the port mouth by a refraction phenomenon: in the deposit trail, Hs increases by about 25% and decreases by 15-20% on either side of the deposit. This causes an increase in energy on the port's breakwaters (mechanical stress), and an increase in Hs about 30-35% in the port mouth, navigation operations (in and out of port) can be therefore more difficult.

CONCLUSION

This study based on water level measurements and numerical simulation during a 1-year return period storm event shows that the contribution of short waves (5-30 s) to the oscillations of Port of Bayonne is low: $Hs_{SW} = 1\ m$ at the river mouth and $Hs_{SW} < 0.15\ m$ in the port. The breakwaters at the port mouth efficiency protect the port against incoming swell and sea waves with a reduction factor of 85% compared to the offshore wave energy. In contrast, a large amount of energy was found in the IG period band (80% of total energy), with a Hs_{IG} reaching maximum values of 0.5 m and 1 m in the channel harbor and the marina respectively. IG waves are generated by oceanic forcing (incident swell). The deposit of dredged material, by a refraction phenomenon, concentrates the energy of incident waves on the port mouth and the breakwaters, which can disturb the ship navigation. It also favors the shoaling of short waves and possibly the generation of IG waves by non-linear interaction phenomenon. As they enter the port, the IG waves propagate freely (without amplification) in the river which acts as a wave guide, and gradually dissipate by friction. However, they conserve enough energy to cause the resonance of the marina (coastal seiche), and to probably excite the moored vessel whose own eigen periods are in the IG period band.

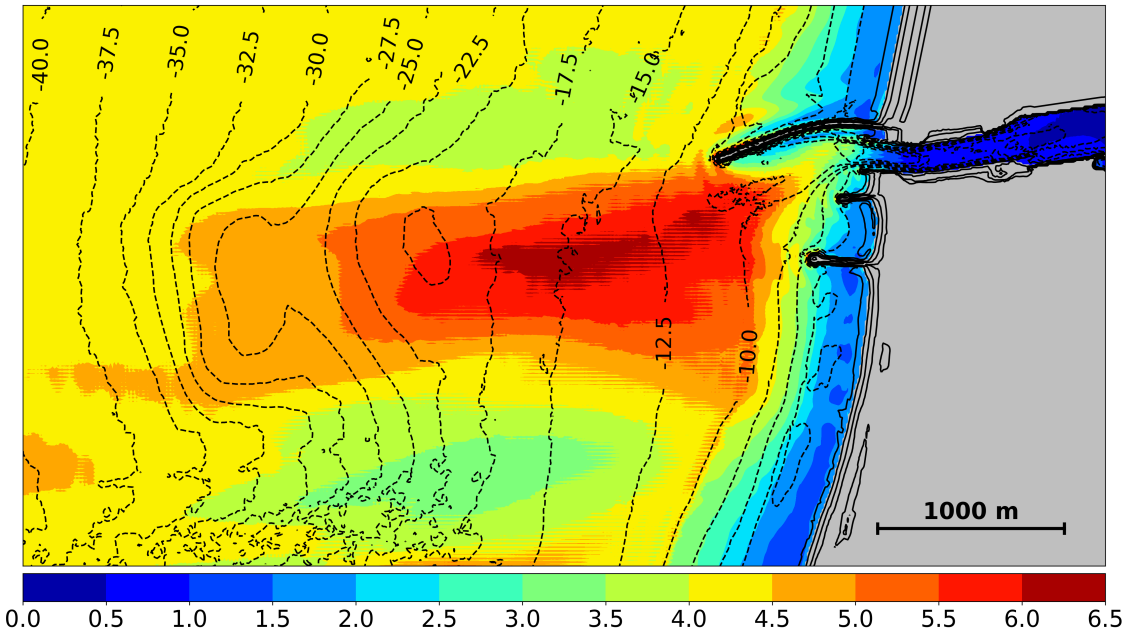

Figure 7: Hs map (m) and contour lines (mCD - dotted lines). Grid resolution = 10 m.

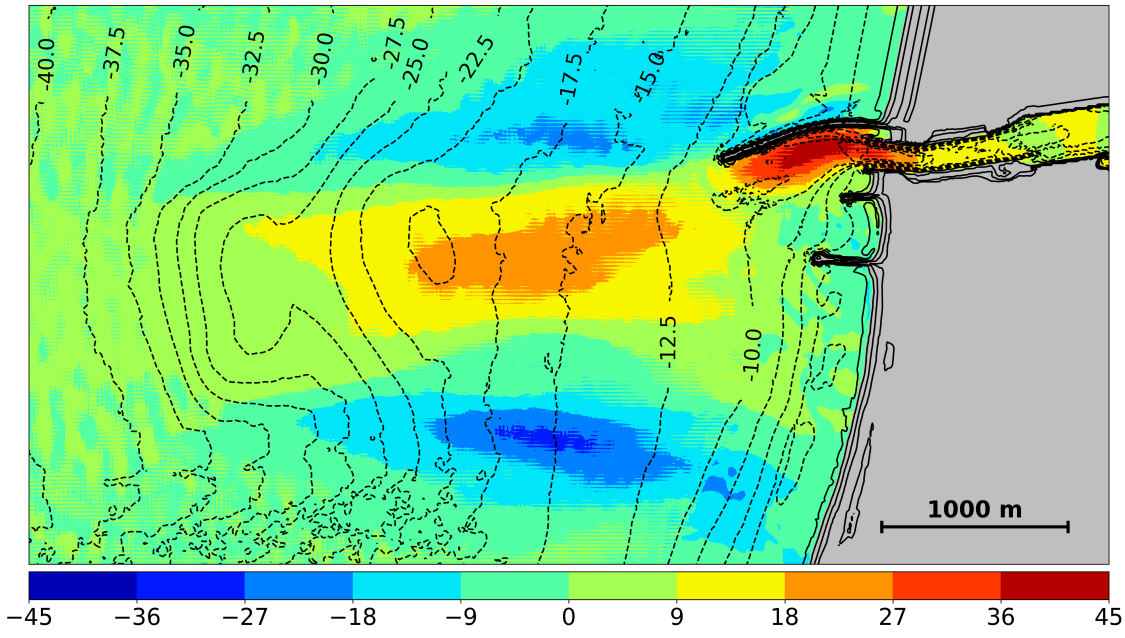

Figure 8: Differences of Hs (%) with and without the deposit of dredged material: positive values are increases.

ACKNOWLEDGEMENTS

The authors thank the technical service of the port of Bayonne for the support provided during the design of the measuring devices. The work is co-funded by the Region Nouvelle Aquitaine (France) and the Hydrographic and Oceanographic Service of the Navy (SHOM, France).

References

S. Abadie, R. Butel, H. Dupuis, and C. Brière. Paramètres statistiques de la houle au large de la côte sud-aquitaine. *Comptes Rendus Geoscience*, 337(8):769–776, 2005.

G. J. Arcement and V. R. Schneider. Guide for selecting manning's roughness coefficients for natural channels and flood plains, 1989.

C. Augris and P. Clabaut. *Cartographie géologique des fonds marins côtiers: exemples le long du littoral français*. Editions Quae, 2001.

J. Berkhoff. Computation of combined refraction—diffraction. In *Coastal Engineering 1972*, pages 471–490. 1973.

X. Bertin, A. de Bakker, A. van Dongeren, G. Coco, G. André, F. Ardhuin, P. Bonneton, F. Bouchette, B. Castelle, W. C. Crawford, M. Davidson, M. Deen, G. Dodet, T. Guérin, K. Inch, F. Leckler, R. McCall, H. Muller, M. Olabarrieta, D. Roelvink, G. Ruessink, D. Sous, Éléonore Stutzmann, and M. Tissier. Infragravity waves: From driving mechanisms to impacts. *Earth-Science Reviews*, 177:774 – 799, 2018. ISSN 0012-8252. doi: https://doi.org/10.1016/j.earscirev.2018.01.002. URL http://www.sciencedirect.com/science/article/pii/S0012825217303239.

P. Bonneton and D. Lannes. Recovering water wave elevation from pressure measurements. *Journal of Fluid Mechanics*, 833:399–429, 2017.

N. Booij, L. Holthuijsen, and R. Ris. The" swan" wave model for shallow water. In *Coastal Engineering 1996*, pages 668–676. 1997.

T. Gierlevsen, M. Hebsgaard, and J. Kirkegaard. Wave disturbance modelling in the port of sines, portugal–with special emphasis on long period oscillations. In *Proceedings International Conference on Port and Maritime R&D and Technology, Singapore, 29-13 October 2001*, 2001.

M. Guerrini, G. Bellotti, Y. Fan, and L. Franco. Numerical modelling of long waves amplification at marina di carrara harbour. *Applied Ocean Research*, 48:322–330, 2014.

L. H. Holthuijsen. *Waves in oceanic and coastal waters*. Cambridge university press, 2010.

J.-J. Lee and X. Xing. Computer modeling for harbor planning and design. In *Handbook of Coastal and Ocean Engineering*, pages 695–722. World Scientific, 2010.

M. S. Longuet-Higgins and R. Stewart. Radiation stress and mass transport in gravity waves, with application to 'surf beats'. *Journal of Fluid Mechanics*, 13(4):481–504, 1962.

O. Nwogu. Alternative form of boussinesq equations for nearshore wave propagation. *Journal of waterway, port, coastal, and ocean engineering*, 119(6):618–638, 1993.

M. Okihiro, R. Guza, and R. Seymour. Excitation of seiche observed in a small harbor. *Journal of Geophysical Research: Oceans*, 98(C10):18201–18211, 1993.

A. B. Rabinovich. Seiches and harbor oscillations. *Handbook of coastal and ocean engineering*, pages 193–236, 2009.

F. Raichlen. Harbor resonance. *Estuary and coastline hydrodynamics*, 1966.

V. Roeber and J. D. Bricker. Destructive tsunami-like wave generated by surf beat over a coral reef during typhoon haiyan. *Nature Communications*, 6:7854 EP –, 08 2015.

V. Roeber and K. F. Cheung. Boussinesq-type model for energetic breaking waves in fringing reef environments. *Coastal Engineering*, 70:1–20, 2012.

V. Roeber, K. F. Cheung, and M. H. Kobayashi. Shock-capturing boussinesq-type model for nearshore wave processes. *Coastal Engineering*, 57(4):407–423, 2010.

G. Symonds, D. A. Huntley, and A. J. Bowen. Two-dimensional surf beat: Long wave generation by a time-varying breakpoint. *Journal of Geophysical Research: Oceans*, 87(C1):492–498, 1982.

S. team et al. Swan user manual. *Delft University of Technology. The Netherlands*, 2007.

E. F. Thompson and L. L. Hadley. Numerical modeling of harbor response to waves. *Journal of coastal research*, pages 744–753, 1995.

R. E. Thomson and W. J. Emery. *Data analysis methods in physical oceanography*. Newnes, 2014.

D. T. Thotagamuwage and C. B. Pattiaratchi. Observations of infragravity period oscillations in a small marina. *Ocean Engineering*, 88:435–445, 2014a.

D. T. Thotagamuwage and C. B. Pattiaratchi. Influence of offshore topography on infragravity period oscillations in two rocks marina, western australia. *Coastal Engineering*, 91:220–230, 2014b.

H. L. Tolman et al. User manual and system documentation of wavewatch iii tm version 3.14. *Technical note, MMAB Contribution*, 276:220, 2009.

W. Van Der Molen, P. Monardez, and A. Van Dongeren. Numerical simulation of long-period waves and ship motions in tomakomai port, japan. *Coastal Engineering Journal*, 48(01):59–79, 2006.